Measurement of Olefin Bond Rotation Barriers in a Series of Vinylaniline Complexes of the Cyclopentadienyliron(II) Dicarbonyl Cation and Their Correlation to Metal−Olefin Bond Asymmetry

Stephen A. Matchett,* Guirong Zhang,† and David Frattarelli‡

Department of Chemistry, Grand Valley State University, Allendale, Michigan 49401

Received July 1, 2004

^{1}H NMR techniques (selective inversion, total line shape analysis, and $T_1\rho$ measurement) have been used to measure the olefin bond rotation rates in a series of compounds of the general formula $CpFe(CO)_2[\eta^2$-$CH_2C(H)NH(p-C_6H_4X)]$, where X = OMe (**4**), H (**6**), CN (**9**), NO_2 (**10**), Cl (**11**), COOMe (**12**). Complexes **4**, **6**, **11**, and **12** enabled the use of all three methods to yield data sets that spanned a wide temperature range and allowed for reliable determination of the thermodynamic activation parameters for olefin bond rotation. When these three methods were combined with a bootstrap statistical analysis of the Eyring plots, it was possible to resolve the small differences in the $\Delta H^{\ddagger}$ values between three of the four complexes. A clear trend is established between increasing electron donation from the aniline ligand and the facilitation of olefin bond rotation. These results are placed in the context of previous work, providing additional experimental evidence that electronic control from the para position of the aniline influences the overlap of the nitrogen lone pair with the adjacent olefinic carbon. This overlap controls the asymmetry in the metal−olefin bond by displacing the Fp^+ moiety away from the nitrogen-bearing carbon, which is reflected in a drop in the $\Delta H^{\ddagger}$ value for olefin bond rotation.

Understanding the factors that control olefin coordination in metal−olefin complexes is important to exploiting the diverse chemistry of these complexes. Bonding in these complexes was originally described by Chatt, Dewar, and Duncanson[1] as a combination of σ donation from the olefin to the metal and a π back-bond from the metal to the π^* orbital on the olefin. This model is generally appropriate for an interaction in which the metal is symmetrically placed along the olefin face. Metal−olefin bonding, however, ranges from a fully symmetric placement of the metal to strongly asymmetric bonding wherein the metal approaches a purely σ interaction with only one carbon of the double bond. Examples from both ends of this continuum were reported by Rosenblum and co-workers for a series of cationic cyclopentadienyliron(II) dicarbonyl (hereafter referred to as Fp) olefin complexes in the early 1980s.[2] Crystal structures reported for complexes **1**−**3** show the effect of increasing π-donation from the β-carbon substituent on the symmetry of the metal−olefin bond.[2] Rosenblum quantified this asymmetry using the parameter δ, where δ = (distance from Fe to C_β) − (distance from Fe to C_α).

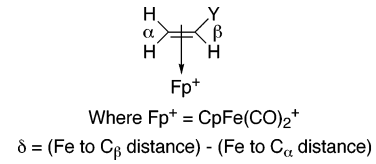

As the π-donor ability of the β substituent increased (Y= H to OMe to NMe_2), the Fp fragment was displaced toward the α-carbon (the value of δ increases). When the donor group possesses a lone pair, the complexes represent points along the resonance continuum between structures I and II.

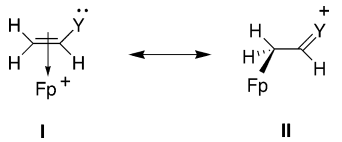

Supported by the calculations of Hoffman and Eisenstein,[3] Rosenblum proposed that the position along this continuum was determined by the ability of a lone pair on the donor to overlap with the developing LUMO that forms on the β-carbon as the Fp fragment is displaced along the olefin face.

Caulton and co-workers[4] recently updated and confirmed the structural characterization of Rosenblum's

* To whom correspondence should be addressed. E-mail: matchets@gvsu.edu.

† Visiting Scientist from the Department of Chemistry, East China Normal University, Shanghai, People's Republic of China 200062.

‡ Undergraduate researcher at Grand Valley State University.

(1) (a) Dewar, M. J. S. *Bull. Soc. Chim. Fr.* **1951**, *18*, C71; *Annu. Rep. Prog. Chem.* **1951**, *48*, 112. (b) Chatt, J.; Duncanson, L. A. *J. Chem. Soc.* **1953**, 2239.

(2) Chang, T. C. T.; Foxman, B. M.; Rosenblum, M.; Stockman, C. *J. Am. Chem. Soc.* **1981**, *103*, 7361.

(3) (a) Eisenstein, O.; Hoffmann, R. *J. Am. Chem. Soc.* **1980**, *102*, 6148. (b) Eisenstein, O.; Hoffmann, R. *J. Am. Chem. Soc.* **1981**, *103*, 4308.

(4) Watson, L. A.; Franzman, B.; Bollinger, J. C.; Caulton, K. G. *New J. Chem.* **2003**, *27*, 1769.

10.1021/om040092r CCC: $27.50
Publication on Web 10/05/2004

heteroatom-substituted Fp^+ olefin complexes[5] and analyzed the metal to olefin bonding asymmetry in the series of Fp^+ olefin complexes $[CpFe(CO)_{2-n}(PH_3)_n(H_2C{=}CHX)]$ (where X = F, OEt, NMe_2 and $n = 0-2$) using density functional theory (DFT) calculations. These calculations supported the conclusion that increased π-donor ability from the heteroatom favors resonance structure II, which dominated in the case of $X = NMe_2$. They also found that as the σ acidity of the metal fragment decreased with increasing PH_3 substitution, both the vinyl fluoride and the vinyl ether moved toward more symmetric metal to olefin bonding. In the case of the vinylamine, however, even the increased electron density from two PH_3 substituents on iron could not significantly alter the extreme asymmetry in its metal−olefin bonding[6] caused by strong π donation from the NMe_2 group.

Recent work in our laboratories has focused on controlling the extent of this asymmetry in Fp−olefin bonding, specifically with nitrogen-substituted olefins. We recently reported[7] synthesizing a series of para-substituted η^2-vinylaniline complexes of the Fp cation (complexes **4**−**10**). Our work demonstrated a correlation

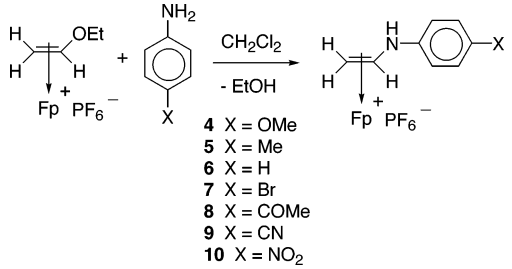

between the ^{13}C shifts of the olefin carbons and the σ_{para} constants for the para substituents on the coordinated vinylaniline. This correlation, and the accompanying X-ray crystal structures of **5** and **8**, gave direct structural evidence[8] for the ability to electronically control the extent of asymmetry in the metal−olefin bonding and hence its position along the continuum represented by resonance structures III and IV. As the electron-

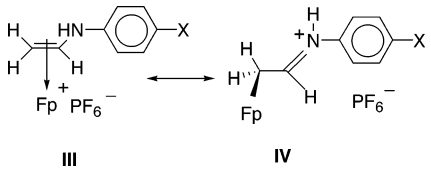

donating properties of the para substituent increased, there was an increased contribution from resonance form IV, leading to a displacement of the Fp^+ fragment toward the α-carbon. Conversely, electron withdrawal from the para position led to an increased contribution from resonance form III.

We contend that substitution at the para position of these vinylanilines is directly influencing the overlap of the nitrogen lone pair with the potential LUMO that develops on the β-carbon as the metal moves across the olefin face.

To strengthen this argument, we sought an additional physical measurement that would assay the relative importance of resonance structure IV in response to electronic changes at the para position. We reasoned that, as the contribution from IV increased, the barrier to rotation about the carbon−carbon bond of the olefin should decrease:

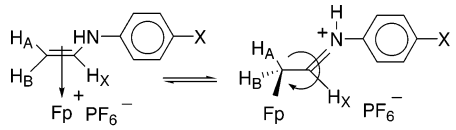

Restricted bond rotation has been described in the literature for many years, with the classic case being amide bond rotation.[9] Because restricted bond rotations often produce exchanges between chemical environments on the NMR time scale, rotation barriers in these systems have been measured using various NMR line-broadening techniques.[10] The preferred method has often been total line shape analysis. This method is most accurate in the vicinity of the coalescence temperature, where the exchange process dominates the line width.[9b] This limits the temperature range of measurable exchange rates, which can lead to inaccuracies in the calculation of activation parameters from regression of the Arrhenius and Eyring plots.[11]

Spin saturation transfer (selective inversion) experiments, originally developed by Forsen and Hoffman,[12] are capable of measuring exchange rates at temperatures well below coalescence. When the ^1H NMR signal of one of the exchange sites is inverted, the system returns to equilibrium magnetization by the normal spin−lattice relaxation, T_1, and by chemical exchange. Curve-fitting routines allow one to separate the exchange rates from the T_1 data, expanding the measurable rate range to include values approximately an order of magnitude smaller than rates obtained through line shape analysis.

In the region of fast exchange, Deverell and coworkers[13] demonstrated that measurement of $T_1\rho$ (spin−lattice relaxation rate in the rotating frame) can be used

(5) They repeated the X-ray structure of $[CpFe(CO)_2(H_2C{=}CHNMe_2)]PF_6$ and solved the structure for $[CpFe(CO)_2(H_2C{=}CHOEt)]PF_6$ in an attempt to overcome the crystal disorder problems encountered with Rosenblum's original structure of $[CpFe(CO)_2(H_2C{=}CHOMe)]PF_6$. Both structures were improved and supported the original conclusions.

(6) Upon comparison of the DFT calculations to the actual X-ray crystal structures for $[CpFe(CO)_2(H_2C{=}CHNMe_2)]PF_6$ and $[CpFe(CO)_2(H_2C{=}CHOEt)]PF_6$, the DFT calculations tended to overestimate the length of the $Fe-C_\alpha$ bond in each case. The authors attribute the discrepancy to the inability of DFT calculations to accurately model weak interactions of this type. Although the bond lengths do not match exactly, the calculations support the trend described.

(7) Matchett, S. A.; Schmiege-Boyle, B. R.; Cooper, J.; Frattarelli, D.; Olson, K.; Roberts, J.; Thommen, J.; Tigelaar, D.; Winkler, F. *Organometallics* **2003**, *22*, 5047.

(8) δ values from these crystal structures were 0.501 and 0.354 Å, respectively.

(9) Stewart, W. E.; Siddall, T. H., III. *Chem. Rev*. **1970**, *70*(5), 517.

(10) (a) Johnson, C. S. *Adv. Magn. Reson.* **1965**, *1*, 33. (b) Sandstrom, J. *Dynamic NMR Spectroscopy*; Academic Press: London, 1982. (c) *Dynamic Nuclear Magnetic Resonance Spectroscopy*; Jackman, L. M., Cotton, F. A., Eds.; Academic: New York, 1975. (d) Kaplan, J. I.; Fraenkel, G. *NMR of Chemically Exchanging Systems*; Academic Press: New York, 1980.

(11) Bain, A. D.; Duns, G. J.; Ternieden, S.; Ma, J.; Werstiuk, N. H. *J. Phys. Chem*. **1994**, *98*, 7458.

(12) (a) Foresen, S.; Hoffman, R. A. *J. Chem. Phys*. **1963**, *39*, 2892. (b) Hoffman, R. E.; Forsen, S. *Prog. Nucl. Magn. Reson. Spectrosc*. **1966**, *1*, 15.

(13) Deverell, C.; Morgan, R. E.; Strange, J. H. *Mol. Phys*. **1970**, *18*, 553.

to extract exchange rates in the range of 10^3-10^6 s^{-1}. Other methods, including the CPMG[14] sequence and more recently offset saturation methods,[15] have also been used in the region of fast exchange.

While each of these techniques allows collection of data in a limited range of rotation rates, the combination of multiple NMR techniques has increasingly been demonstrated[16] to extend the temperature range over which meaningful data can be collected. Combining data sets from selective inversion experiments in the limit of slow exchange, total line shape analysis in the region of coalescence, with offset-saturation techniques in the limit of fast exchange into one Eyring plot, Bain et al. have produced reliable values[17] of the activation parameters for several different bond rotations.

In this paper we report a systematic determination of the activation parameters for rotation about the olefin bond in a series of para-substituted η^2-vinylaniline complexes of the Fp^+ cation using three distinct NMR techniques. To effectively use all three techniques, we also describe the synthesis of two more derivatives in our series: complex **11** (*p*-Cl derivative) and complex **12** (*p*-COOMe derivative). We have employed selective inversion,[18] total line shape analysis, and the $T_1\rho$ experiment to explore the correlation between the activation barriers to olefin bond rotation in these complexes and the electronic properties of the para substituent on the aniline ring. Such a correlation would lend strength to the argument that the para substituent controls the metal−olefin bond symmetry by controlling the availability of the nitrogen lone pair.

Results and Conclusions

The case for restricted olefin bond rotation in these complexes can be seen in their variable-temperature ^1H NMR spectra. The olefin protons in the series of derivatives **4**−**10** all show an A_2X style spectrum at or near room temperature. At these temperatures the two α-protons are equivalent in their coupling to the β-proton, yielding a low-frequency doublet and a high-frequency doublet of triplets (the expected triplet is further split by the adjacent N−H). Figure 1 shows (for **11**, the *p*-Cl derivative) that, as the temperature is lowered, the doublet for the α-protons coalesces and eventually separates into an ABX pattern in the limit of slow exchange.

While total line shape analysis on coupled systems has become more sophisticated,[19] we simplified our treatment by decoupling the β-proton. This simplified the spectrum to yield two peaks (one for each α-proton) at slower rotation rates, collapsing to a singlet in the limit of fast exchange.[20] The comparison of the coupled and decoupled spectra in the fast-exchange region is illustrated for complex **11** in Figure 2.

Dynamic Motions in These Molecules. It is important to establish that the activation parameters measured in this experiment are the direct result of rotation about the $C_\alpha-C_\beta$ bond of the olefin and not some other dynamic process within the molecule. Rotation of the Fp^+ moiety as either classical olefin propeller style rotation or rotation about the $Fe-C_\alpha$ bond in the limit of resonance structure IV must also be considered.[21] We have no doubt that a rotation of the Fp^+ moiety does indeed occur. At room temperature, while most derivatives in the series show an equilibration of the two CO ligands to a single CO peak in the ^{13}C NMR, derivatives **9**, **10**, and **12** show no CO peak. We feel that this is because these latter derivatives are at or near coalescence and the broadening of these peaks does not allow for resolution of these notoriously weak peaks from the baseline.[7] The singlet observed for the other derivatives reflects their lower barrier to CO equilibration, placing them in the limit of fast exchange at room temperature. To confirm this, a series of ^{13}C spectra (acetone-d_6) of complex **4** (*p*-OMe) was taken at temperatures ranging from 5 to −85 °C. Figure 3 shows that as the temperature decreased the singlet seen at room temperature broadened and eventually separated into two peaks in the limit of slow exchange.

Fp^+ rotation (either classic propeller rotation or rotation about the $Fe-C_\alpha$ bond in **IV)** cannot equilibrate either the CO peaks or the geminal protons in the absence of some other molecular motion. It should be noted that classic propeller-style rotation of a symmetrically bound olefin is not a reasonable model in this series, where the ground-state preference for resonance form IV has been previously established in solution by ^{13}C NMR[22] as well in the solid state by the X-ray crystal structures of **2**, **3**, [2] **5**, and **8**.[7] To equilibrate the CO peaks, the molecular motions must generate a plane of symmetry that bisects the CO−Fe−CO angle. In order for the geminal protons to collapse from an ABX system to a clean doublet at room temperature, the cis, trans

(14) (a) Allerhand, A.; Gutowsky, H. S. *J. Chem. Phys*. **1964**, *41*, 2115. (b) Reeves, L. W. In *Dynamic Nuclear Magnetic Resonance Spectroscopy*; Jackman, L. M., Cotton, F. A., Eds.; Academic: New York, 1975, pp 83−130.

(15) (a) Bain, A. D.; Ho, W. P. Y.; Martin, J. S. *J. Magn. Reson.* **1981**, *43*, 328. (b) Bain, A. D.; Duns, G. J. *J. Magn. Reson.* **1993**, *A109*, 56.

(16) (a) Bain, A. D.; Duns, G. J.; Rathgeb, F.; Banderkloet, J. *J. Phys. Chem.* **1995**, *99*, 17338. (b) Bain, A. D.; Hazendonk, P. *J. Phys. Chem. A* **1997**, *101*, 7182. (c) See also ref 10.

(17) Errors in $\Delta H^\ddagger$ of less than 1 kJ/mol and in $\Delta S^\ddagger$ of less than 6 J/(mol K) have been reported.[15] While $\Delta S^\ddagger$ values are often considered suspect, ref 15b presents a case for placing increased faith in $\Delta S^\ddagger$ values obtained by this method.

(18) (a) The authors used a combination of an initial nonselective inversion to determine T_1 values, followed by a selective inversion with curve fitting to determine the exchange rates. This method has been proposed to provide better quantitative kinetic data than the use of the 2-D NMR technique of EXSY.[18b] (b) Bain, A. D.; Fletcher, D. A. *Mol. Phys.* **1998**, *95*, 1091.

(19) (a) Stephenson, D. S.; Binsch, G. *J. Magn. Reson*. **1978**, *32*, 145−152. (b) Binsch, G.; Kessler, H. *Angew. Chem., Int. Ed. Engl*. **1980**, *19*, 411. (c) See also ref 9b, Chapter 3.

(20) In the limit of slow exchange one can begin to freeze out the geminal coupling between the two α-protons. The exchange rates in this temperature range are, however, too slow to be accurately treated by line shape analysis. The geminal coupling constant was included during line shape simulation for accuracy, but the effects are not evident in the temperature range where these simulations were performed.

(21) The authors also considered the possibility of rotation about the imine bond present in systems dominated by resonance structure IV. This was readily dismissed, since such a rotation cannot in itself equilibrate the cis, trans relationships between the α- and β-protons of the coordinated olefin. Second, as the electron-releasing properties of the para substituent are increased, the overlap of the nitrogen lone pair with the β-carbon (to form the imine structure) should increase, increasing the barrier to rotation. The opposite trend is observed, supporting the contention that the data describe rotation of the $C_\alpha-C_\beta$ bond.

(22) Previous work on these complexes show the difference between the ^{13}C chemical shifts for C_α and C_β can be as large as 155 ppm (complex **4**).[7]

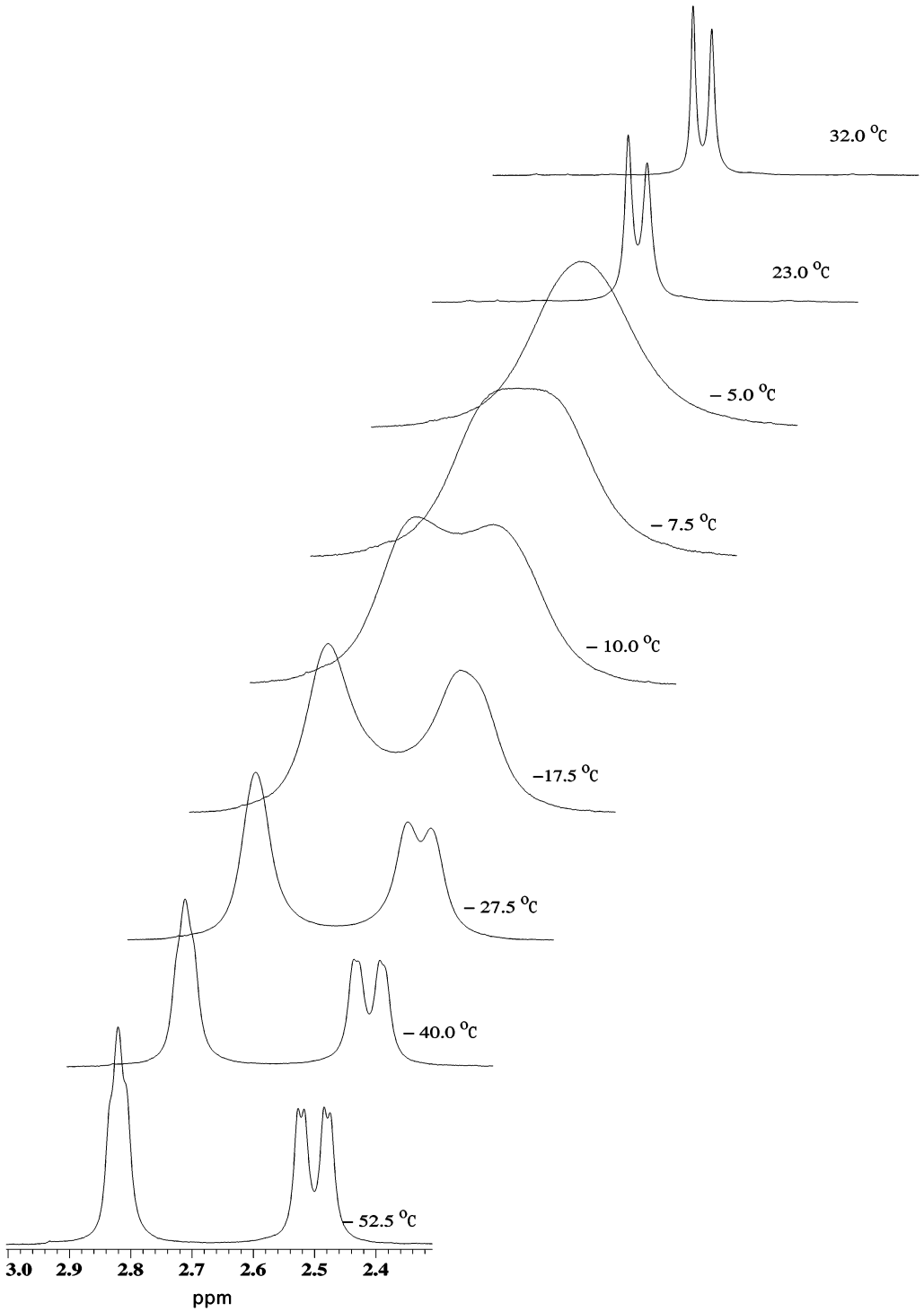

Figure 1. Variable-temperature ^{1}H NMR spectra of the α-protons of complex **11** (*p*-Cl derivative), demonstrating the collapse of the ABX splitting to an A_2B pattern in response to olefin bond rotation.

relationships between the α- and *β*-protons must be equilibrated during the exchange.[23] No rotation of the Fp^+ moiety can be envisioned that would equilibrate either of these positions in the absence of some other dynamic process.

Although rotation of the $C_\alpha-C_\beta$ bond will directly equilibrate the geminal protons, this rotation will not exchange the CO ligands. While the coalescence temperature estimated for this CO exchange (Figure 3) is similar to that reported in Table 1 for $C_\alpha-C_\beta$ bond rotation (−25.0 °C), rotation of this carbon−carbon bond alone will not generate the symmetry necessary to equilibrate the two CO peaks. The previously reported X-ray crystal structures of complexes **5** and **8**[7] both show the Fp^+ moiety to be displaced toward the α-carbon in the solid state. In both cases, one CO is directed under the olefin face toward the *β*-carbon, while the other is directed toward the α-carbon. If only the $C_\alpha-C_\beta$ bond is allowed to rotate, the spatial relationship between each CO and the rest of the molecule will not change. We therefore believe that generation of the symmetry

(23) While the collapse to an A_2B system could also occur if a plane of symmetry developed between the two α-protons, only rotation of the C−C bond could generate such a plane.

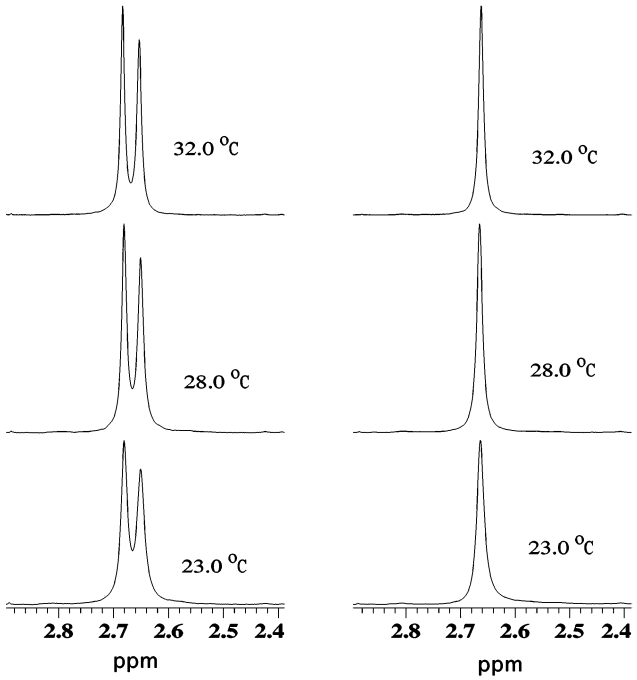

Figure 2. Comparison of the ^{1}H-coupled and ^{1}H-decoupled spectra of the α-protons of complex **11** (*p*-Cl derivative) in the region of fast exchange. The spectra on the left are ^{1}H coupled, while those on the right have been decoupled by irradiation of the *β*-proton.

Table 1. Rotation Rates and the $\Delta G^{\ddagger}$ Values for Olefin Bond Rotation in Complexes 4, 6, and 9−12, As Estimated from the ^{1}H NMR Coalescence Temperature

complex	T_c (°C)	k at T_c (s^{-1})	$\Delta G^{\ddagger}$ from T_c (kJ/mol)
4 (X = OMe), $\sigma = -0.27$	−25.0	185.7	49.6
6 (X = H), $\sigma = 0.00$	−14.0	168.3	52.1
11 (X = Cl), $\sigma = 0.23$	−7.5	158.8	53.6
12 (X = COOMe), $\sigma = 0.45$	2.5	131.7	56.1
9 (X = CN), $\sigma = 0.66$	10.0	123.3	57.9
10 (X = NO_2), $\sigma = 0.78$	15.0	106.7	59.3

plane needed for CO exchange requires both rotation of the Fe−C_α bond (rotation 1 in the drawing below) and rotation of the C_α-C_β bond (rotation 2):

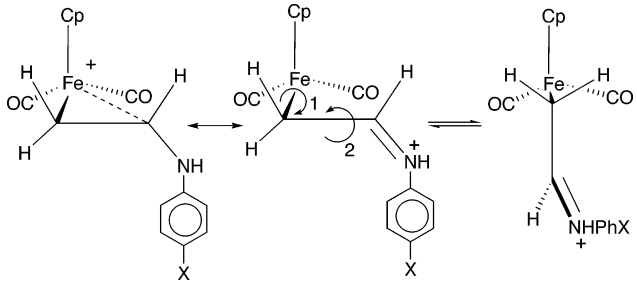

Since both rotations are facilitated by increased contribution from resonance form IV, both are influenced by the electronic properties of the para substituent on the aniline.

While both rotations are necessary to explain the CO exchange, the exchange of the geminal protons only requires the rotation of the C_α−C_β bond. Since Fp^+ rotation is not required to explain the dynamic behavior of the olefin protons, we contend that the data in Tables 1 and 2 directly reflect the influence of the aniline's para substituent on the barrier to C_α−C_β bond rotation.

Measurement of the Activation Parameters. Ideally, rate measurements would be made on each of the complexes (**4**−**10**) from our original ^{13}C correlation study.[7] To make these measurements in all three exchange regimes, one must balance solubility, coalescence temperature (vs solvent freezing/boiling point), and overlap with other peaks in the spectrum. Complex **8** (*p*-COMe) gave only a limited line shape analysis data set due to overlap from the acetyl methyl peak with the α-carbon protons at some temperatures.[24] Complex **9** (*p*-CN) and complex **10** (*p*-NO_2), as expected, had the highest barriers to rotation (more contribution from resonance form III). While these two derivatives gave an excellent data set[25] for the combination of total line shape analysis with selective inversion, the boiling point of the solvent (acetone-d_6)[26] prevented reaching the temperature where rates determined by the $T_1\rho$ experiment are most accurate. To extend the data, two more derivatives of the original series, **11** (*p*-Cl) and **12** (*p*-COOMe), were prepared by reaction of the ethyl vinyl ether compound [$CpFe(CO)_2(CH_2CHOEt)^+PF_6^-$][27] with a slight molar excess of the appropriate para-substituted aniline as the attacking nucleophile (as seen above for **4**−**10**).

Measurement of the coalescence temperature and the approximation of the rotation rates ($k_c = (\pi|\delta\nu|)/\sqrt{2}$)[28] for derivatives **4**, **6**, and **9**−**12** clearly show the influence of the para substituent. This approximation has been demonstrated[29] to give reasonable values for the exchange rates at the coalescence temperature. Table 1 lists these complexes (in order of increasing Hammett σ_{para} value) with their coalescence temperature (T_c), exchange rates at T_c, and $\Delta G^{\ddagger}$ values at T_c. As the electron-donating properties of the para substituent decreased (σ_{para} increased), the T_c value and, hence, the barrier to rotation increased. This reflects a decreasing overlap between the nitrogen lone pair and the *β*-carbon and thus an increasing contribution from resonance structure III. Using this same technique, Rosenblum found[2] the coalescence temperature for **3** (NMe_2 bonded directly to the olefin) to be −60 °C,[30] well below that of **4** (the most electron-rich aniline complex in the current series). Rosenblum's value was determined in CD_2Cl_2 instead of acetone-d_6, which makes the comparison more qualitative.[31] Despite this, it is evident that changing the olefin substituent from a NMe_2 group through the series of increasingly electron-poor anilines raises the

(24) This overlap was extensive for all temperatures for complex **5** (*p*-Me), and no data were collected for this derivative.

(25) The Eyring plot for **9** had an R^2 value of 0.998 for 11 data points. The Eyring plot for **10** had an R^2 value of 0.999 for 15 data points.

(26) Solubility limits the solvent choices to acetone-d_6, methylene-d_2 chloride, or nitromethane-d_3. Methylene-d_2 chloride has similar boiling point limitations, and nitromethane-d_3 freezes above the temperature where these complexes exhibit rates suitable for measurement by selective inversion.

(27) Cutler, A.; Raghu, S.; Rosenblum, M. *J. Organomet. Chem.* **1974**, *77*, 381

(28) (a) Pople, J. A.; Schneider, W. G.; Bernstein, H. J. *High-Resolution Nuclear Magnetic Resonance*; McGraw-Hill: New York, 1959; p 223. (b) $\delta\nu$ is the separation of the peaks (in Hz) in the region of slow exchange, or the peak width at half-height for the peak at coalescence. The latter method was used here, since our simulations showed a slight temperature dependence for $\delta\nu$.

(29) Kost, D.; Carlson, E. H.; Raban, M. *J. Chem. Soc., Chem. Commun.* **1971**, 656.

(30) From this he estimated $\Delta G^{\ddagger}$ at coalescence for rotation of the carbon−carbon double bond to be 43.9 kJ/mol.

(31) A. D. Bain has reported a solvent effect on the internal rotation barriers in furfural.[15b]

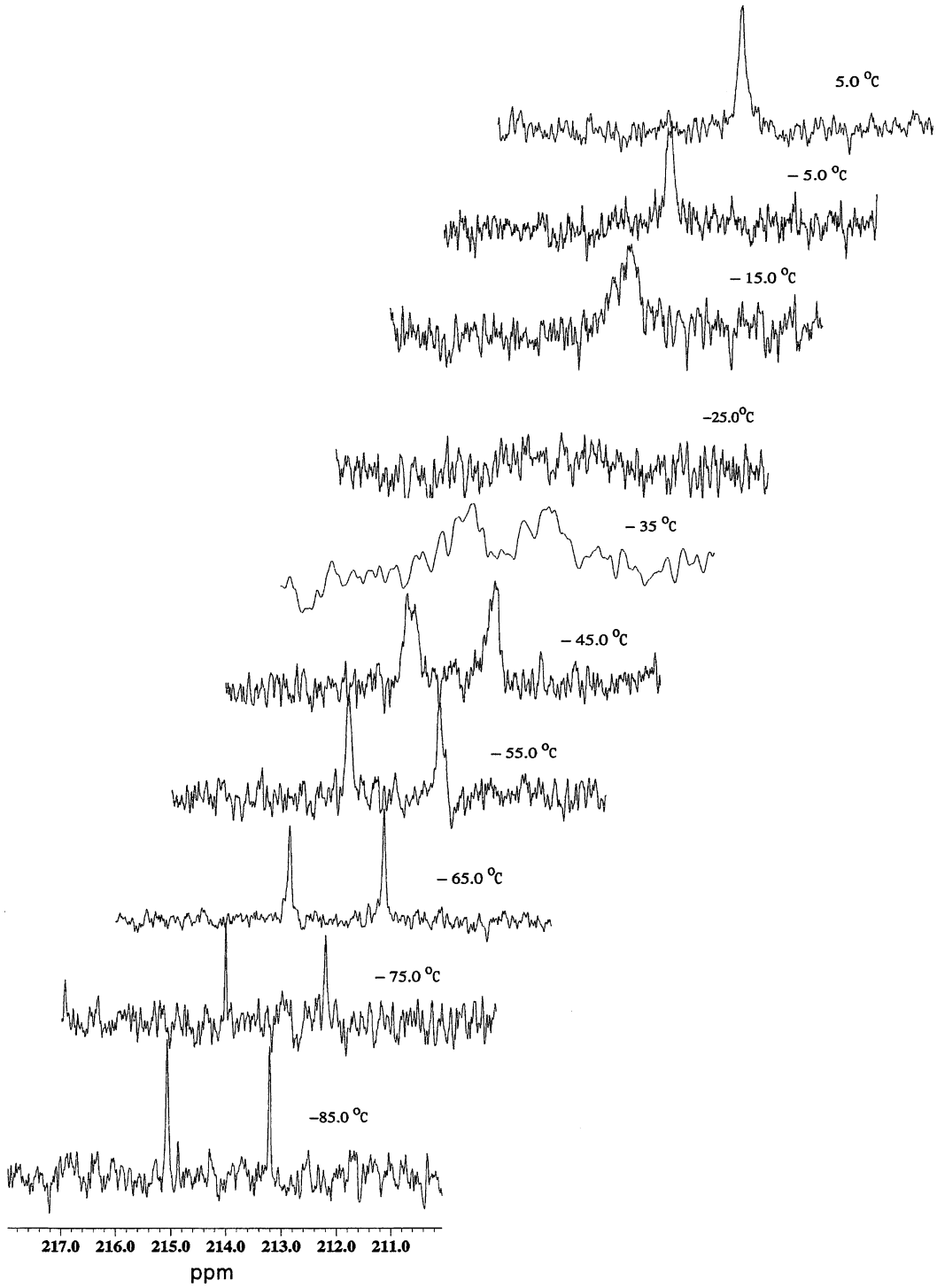

Figure 3. Variable-temperature ^{13}C NMR spectra for the metal carbonyl region of complex **4** (*p*-OMe derivative).

barrier to olefin bond rotation by decreasing the asymmetry in the metal−olefin bonding (a fact previously demonstrated by comparing X-ray crystal structures of **3**, **5**, and **8**).[7]

Although the T_c values described a clear trend, we wished to provide more fundamental activation parameters for this series of complexes. The four derivatives **4** (*p*-OMe), **6** (*p*-H), **11** (*p*-Cl), and **12** (*p*-COOMe) enabled rate measurements to be made using three independent NMR techniques: total line shape analysis, selective inversion, and measurement of $T_1\rho$. Figure 4 gives the Eyring plot for these four derivatives, while Figure 5 gives the Arrhenius plot for the same compounds. Table 2 lists the activation parameters (determined from Figures 4 and 5) for each of the derivatives measured, along with the methods used. Incomplete entries reflect an inability to collect $T_1\rho$ data for complexes **9** and **10**. A preliminary report of some of these data has been recently published in the People's Republic of China.[32]

Comparison of the Data by Method. Table 2 demonstrates that using only total line shape analysis gave the lowest values for the parameters of the bond rotation. Despite excellent linear agreement of the data

(32) Zhang, G. R.; Matchett, S. A.; Dai, L. Y.; Lu, J. X. *J. East China Normal Univ.* **2003**, *2*, 46 (publication in Chinese).

Table 2. Summary of the Activation Parameters for Olefin Bond Rotation in Complexes 4, 6, and 9−12 as a Function of the Various ^{1}H NMR Methods Used[a]

complex (Hammett σ param)	total line shape anal, (TLS)				selective inversion (SI) and TLS combined				$T_1\rho$, SI, and TLS			
	$\Delta H^{\ddagger}$, kJ/mol	$\Delta S^{\ddagger}$, J/(mol K)	E_a, kJ/mol	$\Delta G^{\ddagger}_{298}$, kJ/mol	$\Delta H^{\ddagger}$, kJ/mol	$\Delta S^{\ddagger}$, J/(mol K)	E_a, kJ/mol	$\Delta G^{\ddagger}_{298}$, kJ/mol	$\Delta H^{\ddagger}$, kJ/mol	$\Delta S^{\ddagger}$, J/(mol K)	E_a, kJ/mol	$\Delta G^{\ddagger}_{298}$, kJ/mol
4, X = OMe (−0.27)	40.0 (±0.5)	−38.8 (±2.0)	42.0 (±0.5)	51.5 (±1.1)[b]	39.6 (±1.1)	−39.9 (±4.8)	41.6 (±1.1)	51.4 (±2.5)	43.9 (±1.0)	−21.7 (±4.3)	45.9 (±1.0)	50.4 (±2.3)
6, X = H (σ = 0.0)	37.5 (±0.9)	−57.5 (±3.5)	39.5 (±0.9)	54.6 (±1.9)	45.8 (±0.9)	−24.1 (±3.8)	47.8 (±0.9)	52.9 (±2.0)	46.6 (±0.6)	−20.9 (±2.3)	48.7 (±0.6)	52.8 (±1.3)
11, X = Cl (0.23)	39.6 (±0.7)	-53.0 (±2.7)	41.8 (±0.7)	55.4 (±1.5)	45.5 (±0.9)	−30.3 (±3.6)	47.5 (±0.9)	54.5 (±2.0)	48.1 (±0.8)	−19.4 (±3.2)	50.3 (±0.8)	53.8 (±1.8)
12, X = COOMe (0.45)	45.9 (±1.4)	−37.2 (±5.4)	48.1 (±1.4)	57.0 (±3.0)	54.9 (±0.7)	−3.5 (±2.7)	57.0 (±0.7)	55.9 (±1.5)	55.1 (±0.5)	−2.8 (±2.1)	57.2 (±0.5)	55.9 (±1.1)
9, X = CN (0.66)	52.0 (±0.4)	−21.5 (±1.6)	54.3 (±0.4)	58.4 (±0.9)	54.3 (±0.5)	−12.8 (±1.8)	56.4 (±0.5)	58.1 (±1.0)				
10, X = NO_2 (0.78)	53.4 (±2.8)	−18.5 (±10.1)	55.7 (±2.8)	58.9 (±5.8)	61.6 (±0.8)	10.9 (±3.1)	63.8 (±0.8)	58.4 (±0.1)				

[a] Errors are reported as ±2 standard deviations. [b] Errors on the $\Delta G^{\ddagger}$ values are calculated from the formula $\sigma(\Delta G^{\ddagger}) \approx |\sigma(\Delta H^{\ddagger}) - T\sigma(\Delta S^{\ddagger})|$.[17b]

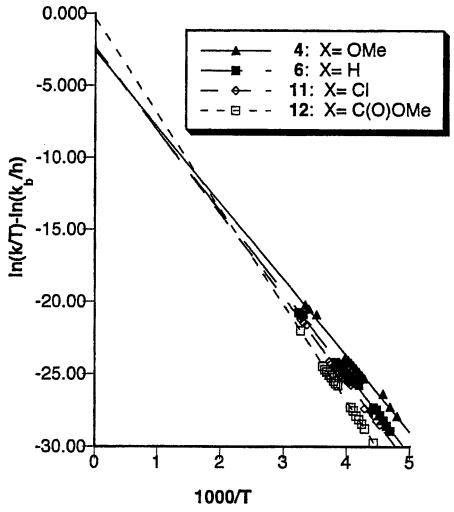

Figure 4. Eyring plot for complexes **4** (*p*-OMe), **6** (*p*-H), **11** (*p*-Cl), and **12** (*p*-COOMe). Data were collected by a combination of selective inversion, total line shape analysis, and spin lock ($T_1\rho$) techniques.

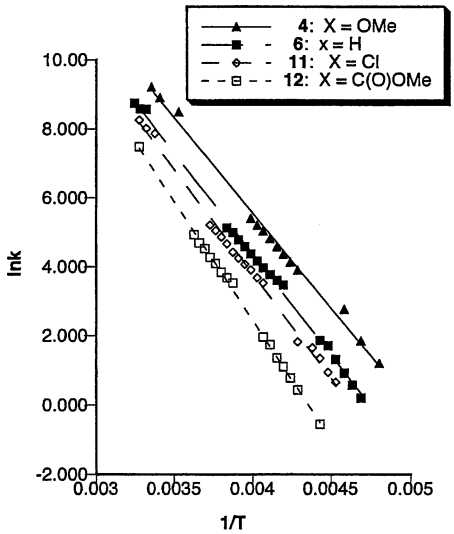

Figure 5. Arrhenius plot for complexes **4** (*p*-OMe), **6** (*p*-H), **11** (*p*-Cl), and **12** (*p*-COOMe). Data were collected by a combination of selective inversion, total line shape analysis, and spin lock ($T_1\rho$) techniques.

in the region of intermediate exchange, each additional NMR method extended the temperature range and acted to refine the values determined for $\Delta H^{\ddagger}$ and $\Delta S^{\ddagger}$. Use of the selective inversion technique extended the data into the region of slow exchange ($k = 0.1-10\ s^{-1}$) and generally acted to increase the values of $\Delta H^{\ddagger}$.[33] Data sets with good linear agreement ($R^2 > 0.99$) for a combination of selective inversion with total line shape analysis were obtained for derivatives **4**, **6**, and **9**−**12**. These data, however did not cleanly distinguish the $\Delta H^{\ddagger}$ values between the various derivatives. Inclusion of the $T_1\rho$ experiment (where possible) gave linear data sets for derivatives **4**, **6**, **11**, and **12** ($R^2 = 0.994$, 0.998, 0.996, and 0.999, respectively) and changed the final values slightly. Full data sets for these derivatives average 16 data points collected by 3 independent methods and span a 10^2-10^4 fold range of rates.

Correlation of Bond Rotation Parameters with the Electronic Influence of the Para Substituent. Table 1 shows that the ^{1}H NMR coalescence temperature for rotation about the olefin bond varies directly with the Hammett σ_{para} value for each of six derivatives. While using only TLS or a combination of TLS and SI to calculate the rotation barriers failed to distinguish some of these six derivatives, extension of this general trend to the $\Delta H^{\ddagger}$ value for bond rotation is reasonable. Inclusion of the $T_1\rho$ data refines these measurements and clearly establishes the trend for **4**, **6**, **11**, and **12** (Table 2). As the electron-donating properties of the para substituent increase, the $\Delta H^{\ddagger}$ value for olefin bond rotation decreases. To establish the significance of the differences between these values, it is important to take a conservative look at the error in their measurement.

The error estimation in these quantities is often based on the standard deviation from the linear fit of the Eyring plot. These have the potential to be an optimistic estimation of the error for such data sets. A normal linear regression treats all points as having an equal significance and uniform error, which may not be the case. If the error for each value of k is known, a more accurate estimation of the error in $\Delta H^{\ddagger}$ or $\Delta S^{\ddagger}$ could be determined using a Monte Carlo resampling fit to the data.[34] The problem lies in the estimation of the error in the individual determinations of k, particularly using

(33) In the case of the *p*-OMe derivative, the numbers were almost identical.

(34) By random sampling from within the error range of each data point (k value) and continuous replotting of the data, a large set of regressions could be produced from the same data set. This would produce a range in the slopes and intercepts to the Eyring plot which would give a more conservative estimate of the overall error in each of the activation parameters.

Table 3. Comparison of $\Delta H^{\ddagger}$ and $\Delta S^{\ddagger}$ Values Obtained for Complexes 4, 6, 11, and 12 by Single Linear Regression of the Eyring Plots versus Multiple Regressions using the Bootstrap Method[a]

	linear regression		bootstrap method	
complex	$\Delta H^{\ddagger}$, kJ/mol	$\Delta S^{\ddagger}$, J/(mol K)	$\Delta H^{\ddagger}$, kJ/mol	$\Delta S^{\ddagger}$, J/(mol K)
4 (X = OMe)	43.9(±1.0)	−21.70(±4.3)	43.8(±1.4)	−22.1(±5.9)
6 (X = H)	46.6(±0.6)	−20.88(±2.3)	47.2(±0.8)	−18.1(±3.4)
11 (X = Cl)	48.1(±0.8)	−19.44(±3.2)	48.1(±1.0)	−19.7(±3.6)
12 (X = COOMe)	55.1(±0.5)	−2.76(±2.1)	54.2(±0.8)	−5.9(±3.4)

[a] Errors are reported as ±2 standard deviations.

the total line shape method. Typically, k values in this range are determined by minimizing the χ^2 value between the experimental and calculated line shapes. Thus, the σ value for each k value is not easily determined. Estimations by visually determining error in line shape methods have been reported with a value of 10%.[16] In the absence of σ values for each k, it is possible to do a similar resampling analysis using the bootstrap method.[35] Here a random set of data points from a given Eyring plot (equal to the number of data points in that curve) are drawn from the original data with the possibility that each point can be drawn more than once. This gives a series of new data sets composed of some fraction of the original points with some points present as duplicates. Each set is then used to create an Eyring plot and regressed to produce values of $\Delta H^{\ddagger}$ and $\Delta S^{\ddagger}$. These are then averaged to give values of $\Delta H^{\ddagger}$ and $\Delta S^{\ddagger}$ with its corresponding σ value. The bootstrap method has been confirmed[36] as a meaningful method for determining the errors in parameter estimations where individual errors are not well defined.[37] We ran a series of 500 such resampled plots on each of our four full data sets. The resulting activation parameters are given in Table 3 along with the more conservative estimation of their uncertainties. Figure 6 shows the relationship between the Hammett σ_{para} constants for each para substituent and the $\Delta H^{\ddagger}$ value for these four compounds determined by the bootstrap method. The more conservative error bars in Figure 6 represent $\pm 2\sigma$ based on applying a bootstrap analysis to the Eyring plots. While errors inherent to the methodology prevent one from cleanly distinguishing between the $\Delta H^{\ddagger}$ values of **6** and **11**, the overall trend remains clear.

An interesting feature of Table 2 is the $\Delta S^{\ddagger}$ values. While complexes **4**, **6**, and **11** all regress to give $\Delta S^{\ddagger}$ values of approximately −20 J/mol K, complex **12** is clearly different at −2.76 J/mol K. This is seen in Figure 4, where the lines are regressed to the origin. Historically, $\Delta S^{\ddagger}$ values obtained by regressing the Eyring plot have been viewed with skepticism, since small changes in the slope can result in a large change in the intercept. The use of combined NMR techniques has expanded the temperature range of the data set and, in doing so, increased confidence in the activation parameters produced. Combining three NMR methods has previously been reported to allow determination of $\Delta H^{\ddagger}$ to within 1 kJ mol^{-1} and $\Delta S^{\ddagger}$ to within 10 J mol^{-1} K.[38] To confirm that the $\Delta S^{\ddagger}$ value for **12** is statistically different for the values seen for the other complexes, we again return to the bootstrap analysis of the error in these values.

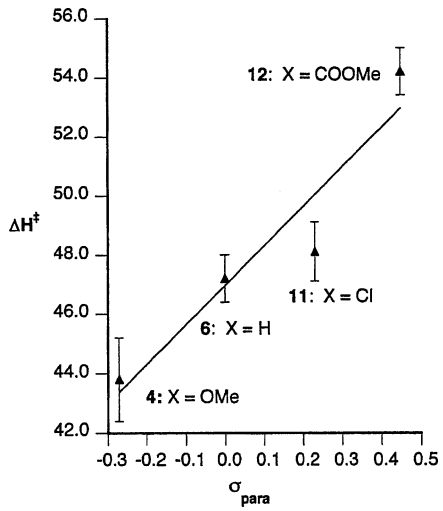

Figure 6. Correlation between $\Delta H^{\ddagger}$ for olefin bond rotation and the Hammett σ_{para} parameter for complexes **4**, **6**, and **9**−**12**.

Even using this conservative estimation of the error (see Table 3 where reported errors are $\pm 2\sigma$), the $\Delta S^{\ddagger}$ value for complex **12** (X = COOMe) differs by approximately 5σ from the next nearest $\Delta S^{\ddagger}$ value.[39] Use of our temperature extended data set in conjunction with conservative error estimation makes a reasonable case that the $\Delta S^{\ddagger}$ value for complex **12** is truly larger than those seen in the other complexes and reflects a difference in the transition state for rotation in that compound. While one would expect the $\Delta H^{\ddagger}$ value to change with the degree of π character in the double bond, it seems at first surprising that the $\Delta S^{\ddagger}$ values are not similar across the series. We contend that the difference is in the ability of the *p*-COOMe group to interact through resonance. In the crystal structure of **8** (*p*-COMe derivative), the molecule was remarkably planar, more so than seen in the structure of **5** (*p*-Me derivative).[7] The latter showed approximately 15° greater rotation in the dihedral angle between the imine (resonance structure IV) and the plane of the aromatic ring. The same dihedral angle in **8** was 178.3°. This planarity would be a reasonable expectation for complex **12**, on the basis of its similarity to **8**. This extra interaction would be disrupted upon rotation, allowing greater rotational freedom and yielding a larger value of $\Delta S^{\ddagger}$. The small exchange data set for **5** does not allow us to produce a $\Delta S^{\ddagger}$ value with the same level of confidence, limiting our argument. Complexes **9** and **10** would also be capable of resonance but yielded only selective inversion and total line shape data sets. Although these smaller data sets are less reliable, regressing the Eyring plot to find $\Delta S^{\ddagger}$ for **9** and **10** gave comparatively larger values of $\Delta S^{\ddagger}$ (−12.8(±1.8) and

(35) Press, W. H.; Teukolsky, S. A.; Vetterling, W. T.; Flannery, B. P. *Numerical Recipes in C: The Art of Scientific Computing,* 2nd ed.; Cambridge University Press: New York, 1992.

(36) Launer, R. L., Wilkinson, G. N., Eds. *Robustness in Statistics*; Academic Press: New York, 1979.

(37) One caveat is offered. The Bootstrap method is best applied when the data set is uniformly distributed across the range of points. Since the three combined NMR methods each have a useable range, there are some gaps in the distribution between these ranges.

(38) Bain, A. D.; Duns, G. J.; Ternieden, J. Ma, Werstiuk, N. H. *J. Phys. Chem*. **1995**, *99*, 17338.

(39) Standard deviation on the difference between the values is calculated as $\sigma_{diff} = \sqrt{(\sigma_{\mathbf{6}}^2 + \sigma_{\mathbf{12}}^2)}$.

10.9(±3.1) J/(mol K), respectively) than were observed with **4** (−39.9(±4.8), **6** (−24.1(±3.8) J/(mol K)) and **11** (−30.3(±3.6) J/(mol K)) when only selective inversion and line shape data sets were used in the analysis. Without the $T_1\rho$ data these numbers are less reliable, but they do support a relationship between resonance from the para position and a larger $\Delta S^{\ddagger}$ value.

In summary, this work demonstrates that there is a direct correlation between the electronic properties of the para group in these η^2-vinylaniline complexes and the NMR coalescence temperature for rotation around the olefin bond. This supports the original hypothesis that the para position is directly influencing the overlap between the nitrogen lone pair and the β-carbon and, hence, controls the position of the iron moiety along the olefin face. Table 2 demonstrates that, despite linearity in the region of coalescence, exclusive reliance on total line shape analysis for calculating activation parameters would lead to considerable underestimation in both $\Delta H^{\ddagger}$ and $\Delta S^{\ddagger}$. Combining three separate NMR techniques over a wide range of temperatures, we have determined the barriers to this olefin bond rotation for four complexes in the series of Fp^+ vinylaniline complexes. This method has allowed us to measure small changes in the $\Delta H^{\ddagger}$ across this series. While the differences in $\Delta H^{\ddagger}$ values were small enough to prevent unambiguous distinction between two members of the series, the correlation clearly seen in the coalescence temperatures is reflected as a reasonable trend in the $\Delta H^{\ddagger}$ values. Work in our laboratories has begun exploring the competition between heteroatom π donors on both the α- and β-carbons and how it influences both the position of the iron moiety along the olefin face and the chemistry of these metal olefin complexes.

Experimental Section

General Procedures. All reactions were carried out under N_2 using standard Schlenk line techniques. Solvents were distilled under a N_2 atmosphere off of appropriate drying and/or deoxygenating reagents (CH_2Cl_2, CaH_2; Et_2O, Na/benzophenone). Acetone-d_6 was dried on 3 Å molecular sieves and vacuum-transferred directly into the NMR tube. NMR spectra were recorded on a JEOL Eclipse 300 at 300.52 MHz for ^1H and 75.57 MHz for ^{13}C. All chemical shifts were referenced to the residual protons in the deuterated solvents. The probe temperature was calibrated using a plot of the chemical shift differences between the OH and the CH_3 resonances of methanol as a function of temperature.[40] Samples were allowed to equilibrate for a minimum of 10 min at each temperature setting, and the probe was then gradient-shimmed prior to collection of each data point. Since all measurements were performed while decoupling the proton on the β-carbon, an initial ^1H NMR spectrum was collected after shimming at a given temperature to accurately determine an irradiation offset value for this proton. Values for the various σ parameters were obtained from ref 41. Samples of the ethyl vinyl ether starting material, $CpFe(CO)_2(CH_2CHOEt)^+PF_6^-$, were prepared by literature methods.[42] All para-substituted anilines were sublimed prior to use. Samples of the known complexes **4**−**10** were prepared by the literature methods.[7] These Fp^+ salts tend to retain solvent (particularly diethyl ether), making elemental analysis more difficult. The new members **11** and **12** of the previously characterized (including analyses)[7] series of compounds were prepared by the same method, and elemental analyses were therefore not performed.

Synthesis of Complexes 11 and 12. These compounds represent two new members of the previously reported[7] series of Fp^+ vinylaniline complexes and were prepared by identical methods. These reactions yielded **11** and **12** in 58% and 70% isolated yields,[43] respectively.

Characterization Data for the *p*-Cl Derivative 11. ^1H NMR (acetone-d_6, 300 MHz): δ 2.67 (br d, 2H, J = 8.0 Hz, olefin CH_2), 5.52 (s, 5H, Cp), 7.55 (s, 4H, aromatic), 8.8 (d of t, 1 H, J_{H-NH} = 12.6 Hz, J = 8.8 Hz, olefin CHN), 10.6 (br d, 1H, J = 10.2 Hz, NH). $^{13}C\{^1H\}$ NMR (acetone-d_6, 75.58 MHz): δ 11.0 (olefin CH_2), 87.3 (CH_{Cp}), 120.8, 130.9, (CH aromatic), 132.5, 137.7 (C aromatic), 158.6 (olefin CHN), 213.6 (Fe−CO) ppm. IR (KBr): 1995, 2049 cm^{-1}.

Characterization Data for the *p*-COOMe Derivative 12. ^1H NMR (acetone-d_6, 300 MHz): δ 2.78 (br d, 2H, J = 8.0 Hz, olefin CH_2), 3.89 (s, 3H, CH_3), 5.62 (s, 5H, Cp), 7.63 (d, 2H, J = 8.5 Hz, aromatic), 8.10, (d, 2H, J = 8.5 Hz, aromatic), 8.9 (d of t, 1 H, J_{H-NH} = 14.3 Hz, J = 9.4 Hz, olefin CHN), 10.5 (br d, 1H, J = 14.0 Hz, NH). $^{13}C\{^1H\}$ NMR (acetone-d_6, 75.58 MHz): δ 13.5 (olefin CH_2), 52.4 (OCH_3), 87.5 (CH_{Cp}), 118.6, 132.2, (CH aromatic), 128.6, 142.8 (C aromatic), 153.2 (olefin CHN), 166.3 (*C*OOMe) ppm. Fe−CO peak(s) not located due to dynamic exchange. IR (KBr): 1996, 2043 cm^{-1}.

^1H NMR Exchange Experiments. Each derivative was prepared as an approximately 0.10 M solution in acetone-d_6 for analysis. Each of the three techniques was carried out on the same sample. Sample tubes were stored in the refrigerator between experiments, where they were stable (under N_2) in solution for weeks.

Selective Inversion. Prior to the selective inversion experiments, the T_1 values for both geminal protons were determined using the standard nonselective inversion T_1 experiment in the JEOL software package.[44] This gives initial T_1 values for use in the nonlinear least-squares fitting of the selective inversion data. The selective inversion experiments were run using a relaxation−$\pi/2$−τ−$\pi/2$−variable delay−$\pi/2$−acquisition pulse sequence with decoupling at the β-proton. The pulse sequence for the decoupling modified version of the standard selective inversion experiment was provided by the software engineers at JEOL (see Acknowledgment). The τ delay value was set at $1/(2\Delta\nu_{A-B})$, where $\Delta\nu_{A-B}$ is the frequency difference between the high-frequency and low-frequency protons on the α-carbon of the molecule being measured. The carrier frequency was set to invert the frequency of the downfield proton. Values for the variable delays were typically chosen to give a set of 10 values evenly spaced between 5 ms and 10 s. The value of the exchange rate was extracted from the best nonlinear least-squares fit of the data using CIFIT,[45] a C version of the SIFIT program written by McClung and Muhandiram.[46] The combination of nonselective and selective inversion experiments has been demonstrated to provide reliable rate data in the limit of slow exchange.[47]

Total Line Shape Analysis. The line shape analysis was performed using MEXITER, an iterative version of Bain's Mexico program.[48] The MEXITER program allows for inclusion

(40) As described in: Braun, S.; Kalinowski, H.-O.; Berger, S. *150 and More Basic NMR Experiments*; Wiley-VCH: New York, 1998; page 136.

(41) March, J. *Advanced Organic Chemistry*; Wiley: New York, 1985; p 244.

(42) Cutler, A.; Raghu, S.; Rosenblum, M. *J. Organomet. Chem.* **1974**, *77*, 381.

(43) These yields are after recrystallization.

(44) Delta NMR Software; JEOL USA Inc. Peabody, MA.

(45) (a) Bain, A. D.; Cramer, J. A. *J. Magn. Reson.* **1996**, *118*, 21. (b) Copies of this program are available from A. D. Bain at the e-mail address bain@mcmaster.ca.

(46) Muhandiram, D. R.; McClung, R. E. D. *J. Magn. Reson.* **1987**, *71*, 187.

(47) Bain, A. D.; Cramer, J. A. *J. Magn. Reson.* **1993**, *103A*, 217.

(48) (a) Bain, A. D.; Dun, G. J. *Can. J. Chem.* **1996**, *74*, 819. (b) The Mexico program is downloadable from http://www.chemistry.mcmaster.ca/~bain/exchange.html. (c) MEXITER was obtained upon request from A. D. Bain, McMaster University.

of the geminal coupling constant as well as the value of the natural line width in the simulation. Experimental spectra were imported into the program as ASCII text files. The spectral simulation was run by refining the ν values for the exchanging peaks[49] until the χ^2 value for the match between the experimental and simulated spectra was minimized.[50] While each derivative displayed some temperature dependence in $\delta\nu$, such dependence is not uncommon[51] and was reliably modeled in MEXITER. Causes may include hydrogen bonding,[52] temperature-dependent changes in the dielectric constant of the solvent,[53] solute aggregation,[54] and dynamic behavior.[55]

***T*$_1\rho$ Experiment.** Prior to the $T_1\rho$ experiments, the T_1 value for the nonirradiated proton was determined using the standard nonselective inversion T_1 experiment in the JEOL software package. The $T_1\rho$ pulse sequence, capable of decoupling the proton on the β-carbon, was provided by JEOL software engineers.[34] In this sequence, the spin−lattice relaxation time in the rotating frame is measured as a function of the spin lock field strength.[56] The decoupler irradiation offset was set to the frequency of the β-proton. The spin lock field attenuator was set at five to six levels, spaced between 15 and 50 dB. The spin lock pulse length was controlled by the pulse program to give 25 evenly spaced values between 0.05 and 10 s. Data were analyzed using the standard JEOL T_1/T_2 data analysis package. The chemical exchange rate was extracted from the $T_1\rho$ value using the graphing method described by Deverell.[11] It should be noted that the $T_1\rho$ experiment may cause heating of the sample if the spin-locking field is too strong. This could cause error in the data if the measured rates are in excess of 10^4 s^{-1}.[11] All rates measured here were well below this threshold except for one, the 25 °C data point for **4**. This was measured to be 10 057 s^{-1}, yet it remained well in line with the rest of the $T_1\rho$ data, as well as the remaining data measured independently by the other methods.

Acknowledgment. We wish to thank the Michigan Space Grant Consortium and the Padnos School of International Studies at Grand Valley State University for their financial support of this work. Thanks are given to Professor A. D. Bain from McMaster University for use of the Mexiter program and his consultations, which helped us greatly in our line shape analysis. His suite of simulation and curve fitting programs were of great value to this work. Thanks are also given to Professor George McBane from Grand Valley State University for his assistance with the Bootstrap error analysis and for his consultations throughout the preparation of this paper. Special thanks are given to Ashok Krishnaswami, Ph.D., Application Chemist, JEOL USA Inc., Peabody, MA. We acknowledge the synthetic contributions of undergraduate researcher Ryan Broekhuizen, who helped in preparing samples of **4** and **6**.

Supporting Information Available: A table of all measured rates by each of the methods. This material is available free of charge via the Internet at http://pubs.acs.org.

OM040092R

(49) These values were always slightly less than the low-temperature exchange limit. The first run started with the low temperature values and each subsequent run used slightly decreased values until the χ^2 value was minimized. Final refined values were used as the starting values for simulating the next higher temperature.

(50) While the MEXITER program will fit the ν values, the exchange rate, and the T_1 values to minimize χ^2, we found more consistent results by manually entering ν values in a series of minimizations.

(51) Reference 10b, p 79.

(52) (a) Maricic, S.; Berg, U.; Frejd, T. *Tetrahedron* **2002**, *58* 3085 (the reference specifically refers to amide hydrogen bonding). (b) Hirayama, F.; Horiuchi, Y.; Utsuki, T.; Uekama, K.; Yamasaki, M. *Jpn. Pharm. Res.* **1993**, *10*, 208.

(53) (a) Golubev, N. S.; Shenderovich, I. G.; Tolstoy, P. M.; Shchepkin, D. N. *J. Mol. Struct.* **2004**, *697*, 9. (b) Takebayashi, Y.; Yoda, S.; Sugeta, T.; Otake, K.; Nakahara, M. *J. Phys. Chem. B* **2003**, *107*, 9847. (c) Garcia-Viloca, M.; Gonzalez-Lafont, A.; Lluch, J. M. *Org. Lett.* **2001**, *3*, 589.

(54) Macchioni, A.; Romani, A.; Zuccaccia, C.; Guglielmetti, G.; Querci, C. *Organometallics* **2003**, *22*, 1526.

(55) It has been proposed that a temperature-dependent change in the relative populations of endo and exo isomers interconverted by propeller style rotation may exist in solution and that this may be causing the observed temperature dependence of $\delta\nu$. This could mean that the observed shifts in the ^{1}H NMR are averages of these two, which may add an additional component to the line broadening. However, there is no evidence for populations of two isomers at −85 °C in the ^{13}C NMR. Given that such temperature dependence is fairly common and can alternatively be caused by many routine factors,[51−54] we do not feel there is much evidence for this complicating factor. The data set is linear as well as collinear with the data obtained by the other methods, which are unaffected by such a possibility.

(56) The parameter setup is described in: Braun, S.; Kalinowski, H.-O.; Berger, S. *150 and More Basic NMR Experiments*; Wiley-VCH: New York, 1998; p 150.